J. Math. Biol. (1994) 32:427–451

Journal of
Mathematical
Biology

Chaos in three species food chains

Aaron Klebanoff[1,*], **Alan Hastings**[2]

[1] Institute of Theoretical Dynamics, University of California, Davis, CA 95616, USA
[2] Division of Environmental Studies, Institute of Theoretical Dynamics, and Center for Population Biology, University of California, Davis, CA 95616, USA

Received 29 October 1992; received in revised form 8 February 1993

Abstract. We study the dynamics of a three species food chain using bifurcation theory to demonstrate the existence of chaotic dynamics in the neighborhood of the equilibrium where the top species in the food chain is absent. The goal of our study is to demonstrate the presence of chaos in a class of ecological models, rather than just in a specific model. This work extends earlier numerical studies of a particular system by Hastings and Powell (1991) by showing that chaos occurs in a class of ecological models. The mathematical techniques we use are based on work by Guckenheimer and Holmes (1983) on co-dimension two bifurcations. However, restrictions on the equations we study imposed by ecological assumptions require a new and somewhat different analysis.

Key words: Chaos – Food chain – Bifurcation – Normal form

1 Introduction

Until recently, theoretical studies of food webs in ecology have, for the most part, focussed on analyses of equilibria (Pimm 1982). The basic rationale behind these studies was the implicit assumption that the communities we observe in nature correspond to stable equilibria of models. However, recent studies have begun to indicate that chaotic dynamics may play an important role in continuous time models in ecology. These studies have all focussed on particular models of very simple food webs, beginning with the work of Gilpin (1979), who examined a Lotka-Volterra model with one predator and two competing prey.

The analysis of the dynamics in almost all these cases has been numerical, without an analytic guide as to the kind of ecological system likely to lead to chaotic dynamics. This is in contrast to the studies of discrete time ecological systems,

* Current address: Department of Mathematics, Rose-Hulman Institute of Technology, 5500 Wabash Avenue, Terre Haute, IN 47803, USA

where it is well known (and can be analytically justified) that the qualitative behavior of the quadratic map and any of the related discrete time logistic models is similar. Chaotic dynamics result for some parameters whenever the density dependence is strong enough, and there is a well developed theory to back up this assertion (Guckenheimer and Holmes 1983). Analytic results on the existence of chaos are important because they can show how chaos arises in a class of models, rather than a particular model. This is particularly important in ecology, where confidence in the exact form of any particular model is weak.

For continuous time models, the analysis is quite a bit more complex. Without seasonality or structure, chaotic dynamics cannot occur unless at least three species are included. Thus, unlike the discrete time case, at least three dimensions must be studied. Therefore, we do not expect as simple a theory that can predict when chaotic dynamics occur in continuous time ecological models as in discrete time models. Our immediate goal here is therefore much more modest. We present an analysis using bifurcation theory that can determine some classes of food chain models where chaos is expected. As far as we know, this is one of the first studies demonstrating the existence of chaotic dynamics in a general class of food chain models.

We will study general three species food chains with the goal being to show the existence of chaotic attractors in biologically reasonable regions of parameter and state space. We will use an approach based on the condimension two bifurcation theory described in Guckenheimer and Holmes (1983). The analysis concentrates on dynamics near an equilibrium state in which the top predator is absent while the lower populations have small amplitude oscillations about an unstable equilibrium. The analysis further focuses on a parameter regime in which several types of bifurcations can occur. Thus, we can study several types of behaviors occurring for a family of food chain models. We will demonstrate our general theory in a specific example: the three species food chain studied numerically by Hastings and Powell (1991), who showed the possibility of chaotic dynamics. We additionally show how this theory applies to more general three species food chains.

The rest of the paper is organized as follows. In Sect. 2, we discuss a very general class of food chain models. All of these models are partially characterized by the existence of a non-trivial equilibrium with the lower trophic species present in the absence of the top predator. In the neighborhood of this equilibrium, we introduce a locally equivalent system which is much simpler to analyze. Section 3 reviews some of the analytic results of a study of a particular family of food chain models with Sect. 4 continuing with numerical results. These sections set the foundation for our study of general food chains by illustrating some of the dynamics phenomena we are searching for. Section 5 as well as the appendices give some of the results of an analysis of the bifurcations about the equilibrium mentioned above. We urge the readers uninterested in the mathematics to skim this to uncover the types of bifurcations which occur and hence the types of population dynamics which may occur. In Sect. 6, we discuss how the analysis can be used to generalize the observed results to more general models. For readers who wish to skip over computations, the paper can be digested without Sects. 2, 3 or 5 except for the end of Sect. 5 on *global bifurcations* which is quite important due to its implications for chaos.

2 General food chain models

A characteristic trait of food chain models is the presence of coupled predator-prey oscillations. Typically, the species higher in the trophic levels oscillate with lower frequency than the species at the bottom trophic levels. Furthermore, in the short term, the species at the bottom of the trophic hierarcy must persist in the absence of the higher species. Hence, in a three species food chain, we expect a non-trivial equilibrium, $(\bar{x}, \bar{y}, 0)$, where we typically expect $(\bar{x}, \bar{y}, 0)$ to have an unstable eigenspace transverse to the xy-plane. Also, the eigenspace of $(\bar{x}, \bar{y}, 0)$ corresponding to the xy-plane should have non-zero imaginary components, and many bifurcations should occur including one which results in an additional non-trivial fixed point with all three species persisting.

The system studied by Hastings and Powell is an example of a more general class of three species models, with the following assumptions (cf. Rosenzweig 1973, Wollkind 1976, and Hastings and Powell 1991), which we will use as the basis for our more general arguments:

(A1) The food chain consists of at least three species, whose population densities vary smoothly as a function of time.
(A2) The species at the bottom of the trophic (nutrient) hierarchy persists in the absence of predation and is generally assumed to have a density dependent growth rate. In other words, at low population densities, the species grow exponentially, while the population densities' growth rate declines at higher densities due to competition for resources.
(A3) The species on the top of the trophic hierarchy are assumed to die off exponentially.
(A4) The only additional factors in the model involve the predator-prey interactions.

Assumption (A2) is a reasonable assumption, while (A3) is a standard "closure" assumption which is necessary to allow for the possibility of stable cycles (which should occur if the model is to be at all realistic). See Steele and Henderson (1992) for a more thorough discussion of the effects of closure types in models.

We begin by considering a general food chain model. The three species food chain shown in Fig. 1 can be modelled as

Fig. 1. A three-species food chain

$$\begin{aligned}
\frac{dX}{dT} &= \hat{D}(X) - F_1(X)Y, \\
\frac{dY}{dT} &= C_1F_1(X)Y - C_2F_2(Y)Z - d_1Y, \\
\frac{dZ}{dT} &= F_2(Y)Z - d_2Z,
\end{aligned} \tag{2.1}$$

where F_i are the functional responses which measure the per predator predation rate as a function of the amount of prey, C_1 and $1/C_2$ are conversion rates of prey into energy for the predator, and $\hat{D}$ represents a density-dependent growth rate function for the lowest prey species. We can rescale this model by letting

$$\begin{aligned}
x &= C_1X\,, \\
y &= Y\,, \\
z &= C_2Z\,, \\
t &= T\,,
\end{aligned} \tag{2.2}$$

and

$$\begin{aligned}
f_1(x) &= C_1F_1(X)\,, \\
f_2(y) &= F_2(Y)\,, \\
D(x) &= C_1\hat{D}(X)\,.
\end{aligned} \tag{2.3}$$

We remark that the f_i's have the same shape as the functional responses. Thus, (2.1) takes the form

$$\begin{aligned}
\dot{x} &= D(x) - f_1(x)y, \\
\dot{y} &= f_1(x)y - f_2(y)z - d_1y, \\
\dot{z} &= f_2(y)z - d_2z.
\end{aligned} \tag{2.4}$$

In order to study bifurcation behavior near $(\bar{x},\bar{y},0)$, we wish to obtain a normal form for (2.4) expanded about $(\bar{x},\bar{y},0)$ so as to simplify the analysis. As shown in Klebanoff (1992), the normal form for any vector field whose linear part is similar to the linear part of (2.4) is of the form

$$\begin{aligned}
\dot{x} &= \omega y + c_1yz + c_2xz + c_3x(x^2+y^2) - c_4y(x^2+y^2) - c_5yz^2 + c_6xz^2 + O(4)\,, \\
\dot{y} &= -\omega x + c_2yz - c_1xz + c_4x(x^2+y^2) + c_3y(x^2+y^2) + c_6yz^2 + c_5xz^2 + O(4)\,, \\
\dot{z} &= c_7(x^2+y^2) + c_8z^2 + c_9z(x^2+y^2) + c_{10}z^3 + O(4)\,.
\end{aligned} \tag{2.5}$$

Here, and from now on, $O(n)$ will denote all monomial terms of degree n and higher. In particular, a normal form for (2.4) expanded about $(\bar{x},\bar{y},0)$ and then shifted to the origin is

$$\begin{aligned}
\dot{x} &= \omega x + c_1yz + c_2xz + c_3x(x^2+y^2) - c_4y(x^2+y^2) - c_5yz^2 + c_6xz^2 + O(4)\,, \\
\dot{y} &= -\omega y + c_2yz - c_1xz + c_4x(x^2+y^2) + c_3y(x^2+y^2) + c_6yz^2 + c_5xz^2 + O(4)\,, \\
\dot{z} &= c_9(x^2+y^2) + c_{10}z^3 + O(4)\,,
\end{aligned} \tag{2.6}$$

where ω and the c_i's depend on $D(x)$, $f_i(x)$, and d_i for $i = 1,2$. This becomes

$$\dot{r} = c_2 rz + c_6 rz^2 + c_3 r^3 + O(4)\,,$$
$$\dot{\theta} = -\omega - c_1 z + c_4 r^2 + c_5 z^2 + O(3)\,,$$
$$\dot{z} = c_9 r^2 z + c_{10} z^3 + O(4)\,, \tag{2.7}$$

in cylindrical coordinates. We note that both c_7 and c_8 are identically zero. While it is not easily apparent what biological assumption results in the absence of the z^2 term in the z-velocity equation (possibly a lack of density dependence in the top predator), it should be clear that c_7 should be zero since otherwise, $z = 0$ would not be invariant and extinct species could materialize "out of nothing".

3 Hastings and Powell's model revisited

We now consider the particular food chain model studied by Hastings and Powell (1991). We will use this model to guide our study of general food chains. Using computer simulations, they showed that their model could exhibit chaotic dynamics for realistic parameter and state values. The model which Hastings and Powell studied was

$$\frac{dX}{dT} = R_0 X\left(1 - \frac{X}{K_0}\right) - C_1 F_1(X) Y$$
$$\frac{dY}{dT} = F_1(X) Y - F_2(Y) Z - D_1 Y$$
$$\frac{dZ}{dT} = C_2 F_2(Y) Z - D_2 Z \tag{3.1}$$

where

$$F_i(U) = \frac{A_i U}{\mathrm{B}_i + U}\,, i = 1, 2 \tag{3.2}$$

represent the Holling type II functional response. As noted by Hastings and Powell, the system can be simplified by choosing the non-dimensional variables to be

$$x = \frac{X}{K_0}\,,$$
$$y = \frac{C_1 Y}{K_0}\,,$$
$$z = \frac{C_1 Z}{C_2 K_0}\,,$$
$$t = R_0 T\,. \tag{3.3}$$

Then, (3.1) becomes

$$\dot{x} = x(1 - x) - \frac{a_1 xy}{1 + b_1 x}\,,$$
$$\dot{y} = \frac{a_1 xy}{1 + b_1 x} - \frac{a_2 yz}{1 + b_2 y} - d_1 y\,,$$
$$\dot{z} = \frac{a_2 yz}{1 + b_2 y} - d_2 z\,, \tag{3.4}$$

where

$$a_1 = \frac{K_0 A_1}{R_0 \mathrm{B}_1},$$

$$a_2 = \frac{C_2 A_2 K_0}{C_1 R_0 \mathrm{B}_2},$$

$$b_1 = \frac{K_0}{\mathrm{B}_1},$$

$$b_2 = \frac{K_0}{C_1 B_2},$$

$$d_1 = \frac{D_1}{R_0},$$

$$d_2 = \frac{D_2}{R_0}, \tag{3.5}$$

are non-dimensional parameters. Hastings and Powell (1991) argued that chaotic dynamics occurred for (3.4) by constructing Poincaré maps and even more convincingly by constructing bifurcation diagrams which show the period doubling route to chaos. We will continue to study the same model which Hastings and Powell studied. We begin by giving some elementary results from the model.

The three species food chain model, (3.4), has six fixed points:

$$(0,0,0), \tag{3.6}$$

$$(1,0,0), \tag{3.7}$$

$$\left(\frac{d_1}{a_1 - b_1 d_1}, \frac{a_1 - b_1 d_1 - d_1}{(a_1 - b_1 d_1)^2}, 0\right), \tag{3.8}$$

$$\left(0, \frac{d_2}{a_2 - b_2 d_2}, \frac{-d_1}{a_2 - b_2 d_2}\right), \tag{3.9}$$

and

$$(\hat{x}_i, \hat{y}_i, \hat{z}_i), i = 1,2, \tag{3.10}$$

where

$$\hat{x}_i = \frac{b_1 - 1}{2b_1} + (-1)^{i-1} \frac{\sqrt{(b_1+1)^2 - \frac{4a_1 b_1 d_2}{a_2 - b_2 d_2}}}{2b_1}, \tag{3.11}$$

$$\hat{y}_1 = \hat{y}_2 = \frac{d_2}{a_2 - b_2 d_2}, \tag{3.12}$$

and

$$\hat{z}_i = \frac{(a_1 - b_1 d_1)\hat{x}_i - d_1}{(a_2 - b_2 d_2)(1 + b_1 \hat{x}_i)}. \tag{3.13}$$

However, there are at most five fixed points in the non-negative octant. The fixed point in the yz-plane cannot occur in the non-negative octant since all of the parameters are positive. Furthermore, the nontrivial fixed point corresponding to the negative sign can only occur in the non-negative octant when d_1 is small enough.

The origin has a two-dimensional stable manifold and a one-dimensional unstable manifold which are the yz-plane and x-axis respectively. Furthermore, the magnitude of the eigenvalues associated with the stable manifold are related only to the death rate parameters d_1 and d_2. The other trivial fixed point, (1, 0, 0) is a sink if $d_1 > a_1/(1 + b_1)$ and otherwise, (1, 0, 0) is a saddle with a two-dimensional stable manifold and a one-dimensional unstable manifold. In other words, if the death rate of predator Y is low relative to the predation rate, then the Y population increases while the X population decreases. The non trivial fixed point, $(\bar{x},\bar{y},0)$ emerges from (1, 0, 0) via a transcritical bifurcation. Finally, the region

$$\mathcal{R} = \{(x,y,z) : 0 \leqq x \leqq 1, y \geqq 0, z \geqq 0\} \tag{3.14}$$

is invariant for the flow induced by (3.4). In other words, the feasible state space is bounded only by extinction and a scaled carrying capacity for the prey. See Klebanoff (1992) for other simple phenomenon and details.

4 Some numerical results and observations

Hastings and Powell (1991) studied the strange attractor shown in Fig. 2. In this section, we will review some other observations made from running numerous simulations of the model in different regions of parameter and state space. Our goal is to point out dynamic phenomena that we can uncover in a study of general food chains which would indicate the presence of chaos in a class of models. To begin, we note that (3.4) has non-trivial dynamics in the absence of the top predator (i.e., when $z = 0$.) In the next section, we compute the conditions for a Hopf bifurcation to occur in the xy-plane and thus prove that a limit cycle emerges from $(\bar{x},\bar{y},0)$ in the xy-plane (e.g., see Fig. 3). We also see Hopf bifurcations occurring in the positive octant off of the non-trivial fixed point $(\hat{x}_1,\hat{y}_1,\hat{z}_1)$. (At the parameter values which we studied, $(\hat{x}_2,\hat{y}_2,\hat{z}_2)$ remained outside of the positive octant.)

An interesting chain of events occurs leading up to and following a Hopf bifurcation which ultimately results in the chaotic attractor shown in Fig. 2. Any of the six parameters can act as a bifurcation parameter. However, we chose b_1 since this is the one used by Hastings and Powell (1991). The reader should note from (3.5) that an increase in b_1 corresponds to an increase in the carrying capacity of prey species X. Also, an increase in b_1 results in a decrease in per predator Y predation of prey X. Furthermore, as b_1 increases, the functional response of predator Y on prey X acts to destabilize the system allowing for more complicated dynamics. For small b_1, there is no limit cycle in the xy-plane, and $(\bar{x},\bar{y},0)$ is a saddle with a two-dimensional stable manifold (the xy-plane) and a one-dimensional manifold transverse to the xy-plane. Because $(\hat{x}_1,\hat{y}_1,\hat{z}_1)$ is a sink, there is a saddle connection from $(\bar{x},\bar{y},0)$ to $(\hat{x}_1,\hat{y}_1,\hat{z}_1)$. At this stage, in the presence of the top predator, the population sizes readily move towards $(\hat{x}_1,\hat{y}_1,\hat{z}_1)$. As b_1 increases, a bulge forms around the heteroclinic orbit as shown in Fig. 4. As b_1 increases further, the Hopf bifurcation occurs in the xy-plane (so that the interactions between species X and Y become oscillatory) and the bulge opens up on the bottom and connects to the

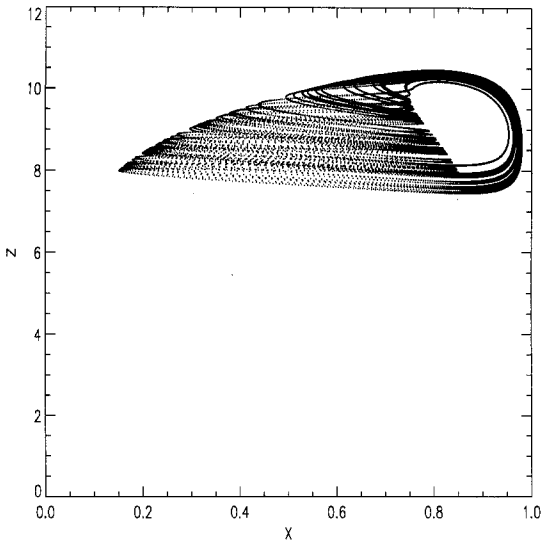

Fig. 2. A strange attractor for the food chain model with $a_1 = 5$, $a_2 = 0.1, b_1 = 3, b_2 = 2, d_1 = 0.4$, $d_2 = 0.01$

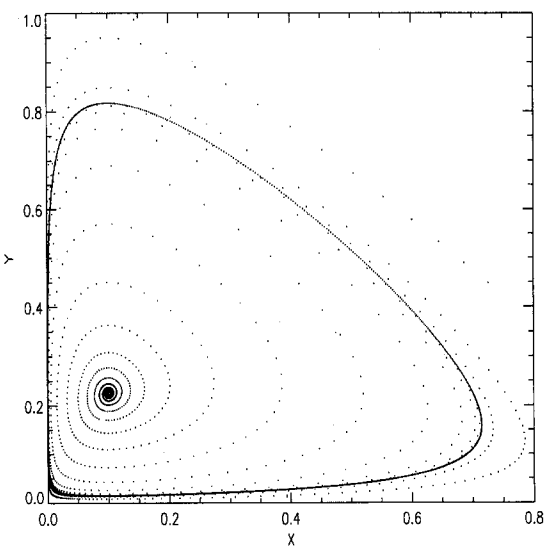

Fig. 3. A limit cycle in the xy-plane for $a_1 = 5, a_2 = 0.1, b_1 = 2.5, b_2 = 2$, $d_1 = 0.4, d_2 = 0.01$

planar limit cycle. At this point, there is an attracting tube on which trajectories wind from near the xy-plane up to the fixed point, $(\hat{x}_1, \hat{y}_1, \hat{z}_1)$. Next, as b_1 grows larger still, the Hopf bifurcation occurs off of $(\hat{x}_1, \hat{y}_1, \hat{z}_1)$. Finally, as b_1 increases further, the limit cycles period double and continue through a sequence of period doubling bifurcations arriving at the attractor shown in Fig. 2. The tube mentioned earlier emanates from the limit cycle in the xy-plane which persists throughout the period doubling route to chaos. Furthermore, the bottom of the "tea-cup" attractor is part of this tube.

There is evidence of a second route to chaos. For certain parameter values, there is a saddle-type limit cycle with a two-dimensional stable manifold and a one-dimensional unstable manifold at the bottom of the attractor. An example is shown

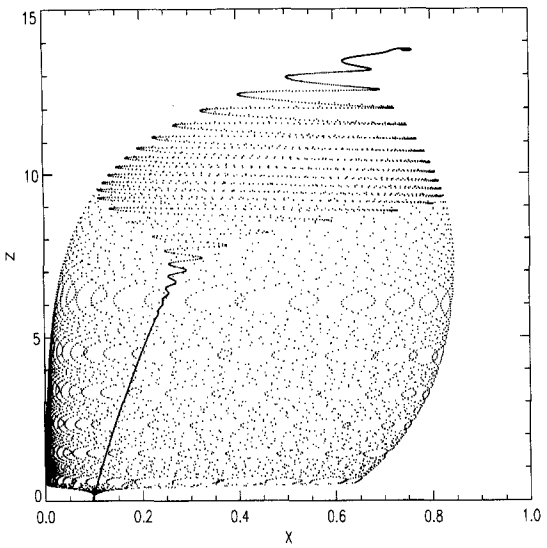

Fig. 4. A "tube" forms as b_1 increases. Here $b_1 = 2$ while the other parameters are fixed at $a_1 = 5$, $a_2 = 0.1, b_2 = 2, d_1 = 0.4, d_2 = 0.01$

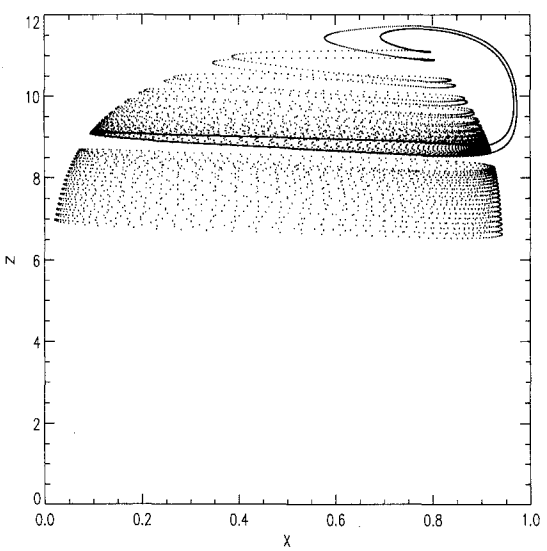

Fig. 5. A saddle limit cycle at the rime of the "tea-cup" attractor. Trajectors spiral away (both above and below) from the limit cycle. The parameters used were $a_1 = 5, a_2 = 0.1$, $b_1 = 3, b_2 = 2, d_1 = 0.3$, $d_2 = 0.01118$

in Fig. 5. It seems likely that a Sil'nikov bifurcation of limit cycles rather than fixed points may occur. At this time, we only conjecture this since it is difficult to prove that there is a homoclinic orbit of limit cycles. This result suggests that the strange attractor may be a torus stretched and wrapped upon itself for these parameter values.

There are many other interesting dynamics occurring. For example, if the death rate of the top predator is increased, then the maximum population size of the top predator depends on its initial size relative to an unstable threshold. This results from a saddle-node bifurcation of limit cycles on the "tube" as shown in Fig. 6. Trajectories wind down the tube between the limit cycles, and wind up it outside of the limit cycles. As the death rate of the top predator continues to increase, the

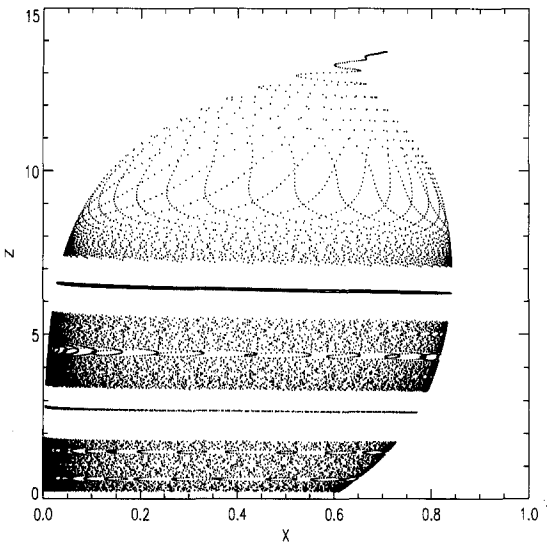

Fig. 6. Saddle-node bifurcation of limit cycles. We let d_2 be the bifurcation parameter with the other parameters all held constant. When $d_2 = 0.01$, there are no limit cycles; as d_2 increases to $d_2 = 0.011$, two limit cycles appear. Flow decreases in z between the limit cycles, and increases in z otherwise. Here, the "tube" is shown "broken" by the limit cycles

limit cycle corresponding to a lower top predator density crosses through the limit cycle in the xy-plane. In other words, a transcritical-type bifurcation of limit cycles occurs.

The following sections are devoted to showing by more rigorous means that the behavior described here really occurs. The most fundamental idea behind our method lies in the fact that biological systems oscillate. Due to this fact, we can make full use of the normal form theorem to find a normal form which is suitable for a change to cylindrical coordinates. In fact, we can write (3.4) expanded about $(\bar{x},\bar{y},0)$ in cylindrical coordinates with the vector field independent of the azimuthal term. As a result, it will suffice to study the resulting system in the rz-plane. Then, for example, fixed points off the z-axis will correspond to limit cycles in (3.4), while fixed points on the z-axis will correspond to fixed points in (3.4). Thus, in order to obtain dynamics such as those discussed here, we will have to have three fixed points on the z-axis: one must be the origin which corresponds to $(\bar{x},\bar{y},0)$, and the other two corresponding to $(\hat{x}_i,\hat{y}_i,\hat{z}_i)$. We must also have a fixed point on the r-axis corresponding to the limit cycle in the xy-plane, and at least two more fixed points in the positive quadrant of the rz-plane to correspond to the limit cycles we have seen in the full system. We further point out that with all of the fixed points given above for the planar system, the conditions for the existence of heteroclinic and homoclinic loops are at least partially satisfied. We will hope to determine the existence of at least one of these phenomenon since the existence of these loops implies horseshoe dynamics for the full system.

5 The normal form analysis

We refer the reader to Appendix A for the normal form calculation. The analysis is local in both parameter and phase space, near the equilibrium point,

$$(\bar{x},\bar{y},0) = \left(\frac{d_1}{a_1 - b_1 d_1}, \frac{a_1 - b_1 d_1 - d_1}{(a_1 - b_1 d_1)^2}, 0\right), \tag{5.1}$$

and the parameter values that lead to a linearization where all the eigenvalues have zero real part. Due to the oscillations inherent in the system, we are able to reduce the system of study to a planar one using cylindrical coordinates and dropping the angular term. Thus, the system of study is

$$\begin{aligned} \dot{r} &= \gamma_1 rz + \gamma_2 rz^2 + \gamma_3 r^3 , \\ \dot{z} &= \gamma_4 r^2 z + \gamma_5 z^3 , \end{aligned} \tag{5.2}$$

where the coefficients are given in Appendix A.

We will now proceed to study the dynamics of (5.2) in the rz-plane. The reader should recognize that the equation for the z-component (the top predator's population size) of the vector field is still representative of the z-component of the vector field in (3.4). The new state variable r is a scaled measure (due to the transformations) of the square root of the sum of the squares of each of the lower trophic species densities. It is close enough to think of an increase in r as an increase in the sum of x and y. Once again, we note that fixed points in the rz-plane with $r > 0$ will correspond to limit cycles for the full system. The reader should note immediately that (5.2) has only the trivial fixed point which corresponds to $(\bar{x}, \bar{y}, 0)$ in (3.4) which corresponds to the absence of the top predator. This makes sense since (5.2) represents dynamics on the center manifold of $(\bar{x}, \bar{y}, 0)$. We will be interested in studying perturbations of (5.2) which then represent the different types of dynamics which can occur for the full system near this bifurcation. We start off, however, by determining the behavior of (5.2) and thus the dynamics of the full system (3.4) in a neighborhood of $(\bar{x}, \bar{y}, 0)$ at bifurcation.

Rescale

To reduce the number of cases we need to study, we rescale (c.f. Guckenheimer and Holmes 1983) by letting $\bar{r} = \alpha r$ and $\bar{z} = \beta z$ to obtain,

$$\begin{aligned} \dot{\bar{r}} &= \frac{\gamma_1}{\beta}\bar{r}\bar{z} + \frac{\gamma_2}{\beta^2}\bar{r}\bar{z}^2 + \frac{\gamma_3}{\alpha^2}\bar{r}^3, \\ \dot{\bar{z}} &= \frac{\gamma_4}{\alpha^2}\bar{r}^2\bar{z} + \frac{\gamma_5}{\beta^2}\bar{z}^3 . \end{aligned} \tag{5.3}$$

By letting $\alpha^2 = -\gamma_3, \beta = \gamma_1$, dropping the bars and letting $a = \gamma_2/\beta^2, b = -\gamma_4/\alpha^2$, and $c = -\gamma_5/\beta^2$, we obtain

$$\begin{aligned} \dot{r} &= rz + arz^2 - r^3 , \\ \dot{z} &= -br^2 z - cz^3 , \end{aligned} \tag{5.4}$$

with a arbitrary and b and c necessarily positive real numbers. One should note that we are assuming that $\gamma \neq 0$. Guckenheimer and Holmes (1983) have done a fairly complete unfolding analysis for a general vector field with the Jacobian matrix in (A.10). They studied (2.5) in cylindrical coordinates by concentrating on the lowest order terms and required that c_2, c_7 and c_8 were non-zero. In our case, we have $c_2 \neq 0$ while $c_7 = c_8 = 0$. As mentioned earlier, the absence of c_7 is no surprise since in the absence of the top predator, it must remain extinct. As a result of these different constraints, we cannot follow the analysis given in Guckenheimer

and Holmes. We do, however, profit from their work and follow the same basic outline for analysis.

Isoclines for the vector field in normal form

A useful tool for determining the phase portraits is to utilize isoclines, i.e., curves of constant slope. In particular, the zero isoclines or *nullclines* show where the vector field points parallel to one of the axes. Additionally, the points of intersection of nullclines for the different state variables are the fixed points of the vector field. For (5.4), it is clear that $r = 0$ and $z = 0$ are nullclines corresponding to $\dot{r} = 0$ and $\dot{z} = 0$ respectively. The only other nullcline corresponding to $\dot{r} = 0$ is the conic section

$$4a^2\left(z + \frac{1}{2a}\right)^2 - 4ar^2 = 1, a \neq 0\,. \tag{5.5}$$

The nullcline given in (5.5) is a hyperbola when $a > 0$, and an ellipse when $a < 0$. If $a = 0$, the nullclline corresponding to $\dot{r} = 0$ is the parabolic nullcline,

$$z = r^2\,. \tag{5.6}$$

See Fig. 7 for a comparison of the dynamics near $(0, 0)$ with the different nullclines.

We can now briefly describe the dynamics of (3.4) near $(\bar{x}, \bar{y}, 0)$ at bifurcation. From Fig. 7, it is clear that trajectories near $(\bar{x}, \bar{y}, 0)$ spiral towards it. It is also interesting to note that the bulge which we noticed from numerical studies is also found from the normal form computation. We also note that local to the origin, there is no topological difference between the phase portraits in Fig. 7. Thus, on the center manifold, the phase portrait near $(\bar{x}, \bar{y}, 0)$ must look as is shown in Fig. 8.

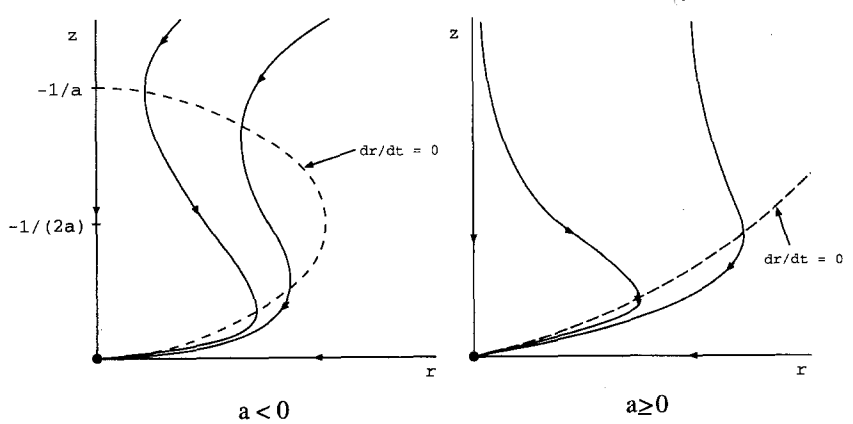

Fig. 7. When $a > 0$, the nullclines are the axes and a branch of a hyperbola. When $a = 0$, the non trivial nullcline is a parabola. (We combine $a = 0$ and $a > 0$ into one graph for compactness since they appear similar.) When $a < 0$, non trivial nullcline is an ellipse. The reader should note that for all a, the nullclines local to the origin appear the same

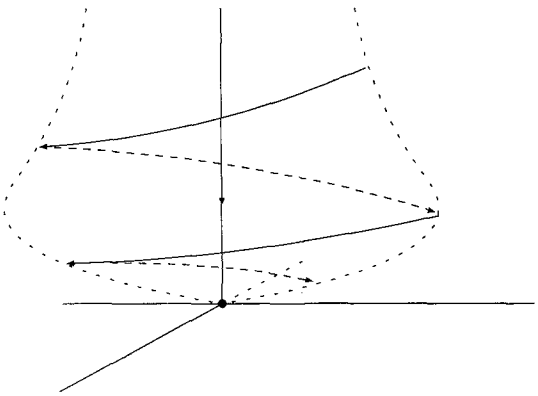

Fig. 8. By adding the affect of the az imuthal term to the planar system, we see how the flow looks near $(\bar{x}, \bar{y}, 0)$ at bifurcation in the full system

Determine the unfolding

We now wish to unfold the vector field in (5.4) in order to capture dynamics of the original system in terms of the simpler system in normal form. We do not attempt to nor claim to attain a universal unfolding. In fact, we do not want a universal unfolding since we have biological factors to consider which restricts us from studying all possible perturbations of (5.4). In particular, it is necessary that $z = 0$ be invariant (i.e., if the top predator is absent, it must remain so), so we must not introduce any term in the z equation independent of z. Furthermore, the unfolding should exhibit global bifurcations. Otherwise, we could not account for the dynamics of the full system. A global bifurcation in the plane is associated with the dynamics of the horseshoe map and implies exponential expansions and contractions in a neighborhood of the saddle. The planar analogy to a Sil'nikov-like phenomenon discussed in Sect. 4 is a limit cycle growing into a homoclinic loop and "exploding" through it leaving no loop or limit cycle behind. With all of this in mind, we introduce an unfolding of (5.4) given by

$$\begin{aligned} \dot{r} &= \mu_1 r + rz + arz^2 - r^3 , \\ \dot{z} &= \mu_2 z + \mu_3 z^2 - br^2 z - cz^3 . \end{aligned} \tag{5.7}$$

Again, we stress that this does not yield a universal unfolding of (5.4). However, we will show that the three parameter unfolding in (5.7) is sufficient for finding limit cycles and homoclinic bifurcations in the rz-plane, i.e., corresponding to the types of solutions previously found numerically by Hastings and Powell (1991) and Klebanoff (1992) for the full system with three species.

Analysis of unfolded system

The analysis which we were able to carry out is quite standard and cumbersome. However, the results of the analysis are quite useful. We were able to determine all of the local behavior in the full system from the local analysis of (5.7). For example, we found saddle-node bifurcations of limit cycles nearly parallel to the xy-plane (i.e., fixed oscillations at the lower trophic levels with a steady population size for the top predator). In cylindrical coordinates, this would appear as a saddle-node bifurcation of fixed points off of the rz axes. From the analysis, we were

able to show which limit cycle was stable and which was not. We show several of our results with biological implications in Appendix B, and we refer the reader to Klebanoff (1992) for more details.

Of the elementary bifurcations which occurred, the Hopf bifurcation was–in some ways–the most important. It is important to realize that a Hopf bifurcation in the rz-plane implies the emergence of quasiperiodic behavior in the full system. This is especially important since this is the first phenomenon which we have not determined numerically, but that must occur. It should not be a big surprise if invariant tori exist in the full system. We remind the reader that the "tea-cup" attractor is quite reminiscent of the Sil'nikov phenomenon, but about a limit cycle rather than a fixed point. Near a Sil'nikov-type bifurcation for limit cycles, there is a near homoclinic connection for the limit cycle which implies that the unstable manifold of the limit cycle loops around and onto the stable manifold of the limit cycle which pulls it back down towards the limit cycle. Since this is only close to (not at) bifurcation, the unstable manifold continues past the limit cycle on its second time around by winding around the first loop in order to stay close to and wind back onto the stable manifold. The reader should compare the dynamics of the "tea-cup" attractor (see Fig. 2) to the dynamics given by Sil'nikov's phenomenon. While this does not yield the same behavior as quasi-periodic flow, the shape of the trajectories on the phase portrait are similar. The flow on the "tea-cup" attractor can be thought of as a tube which is stretched as it reaches its peak (thus the thinning), then greatly compressed so as to lose its thickness as it moves down the handle, and the flattened handle can wrap back around the tune, repeating the process over and over again resulting in chaotic dynamics.

Global bifurcations and chaos

One type of global bifurcation is the homoclinic bifurcation. This occurs when the stable and unstable manifolds of a saddle point cross away from the saddle point. Because we are considering smooth vector fields, this must imply that the stable and unstable manifolds coincide forming a closed curve. In the planar system, (5.7), since the r-axis and z-axis are both invariant for the flow, the homoclinic bifurcation can only occur off of the axes. Furthermore, since there are no more than two non-trivial fixed points, the homoclinic bifurcation can occur only when they are both present with one as a saddle, and the other necessarily a node which must be contained inside the homoclinic loop. We locate the global bifurcations by studying the myriad of possible intersections of the nullclines (shown in Fig. B.1) and then we demonstrate via a numerical study that a homoclinic bifurcation occurs by visually showing how the separatrices change via the bifurcation. Figure 9 shows a typical homoclinic bifurcation for (5.7).

We now discuss the implications of the homoclinic bifurcation for the full system. At bifurcation, the homoclinic loop appears as a kinked torus in three-space for the full system. However, the flow is not toroidal because of the saddle-type limit cycle. The homoclinic connection is structurally unstable and thus will break up under perturbation. The simpliest way to study this system under perturbation is to create a Poincaré map which is easily found by cutting the flow by the half-plane Poincaré section, $\theta = 0$. Then, the saddle limit cycle and its homoclinic connection appear exactly the same as the phase portrait for the flow. However, we are now

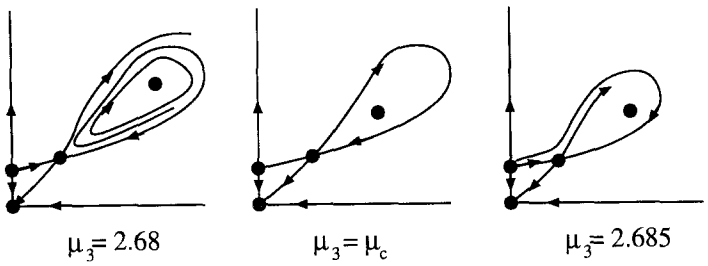

Fig. 9. A homoclinic bifurcation for $2.680 < \mu_3 < 2.685$ with the other parameters set at $a = 0.75, b = 1, c = 0.1, \mu_1 = -0.75, \mu_2 = -1.5$

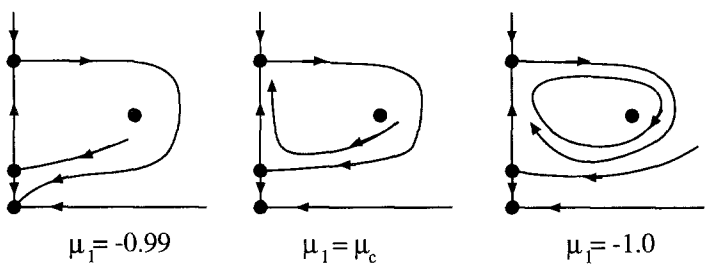

Fig. 10. If we fix $\mu_2 = -1, \mu_3 = 4, a = 0, b = 5.75, c = 1$ and let μ_1 be the bifurcation parameter, then a heteroclinic bifurcation occurs for μ_1 between -1 and -0.99

studying a discrete system. Thus, we expect under perturbations for the stable and unstable manifolds to cross transversely resulting in horseshoes near the saddle. As a result, the full system must also break up under perturbation with chaotic dynamics near the saddle limit cycle. In other words, we expect the full system to exhibit chaotic dynamics where the unfolding is near a homoclinic bifurcation.

We have also remarked that heteroclinic loops in the rz-plane imply horseshoe type dynamics for the full system. Klebanoff (1992) shows that the only possible configuration of a heteroclinic orbit for (5.4) is as shown in Fig. 10. Guckenheimer and Holmes (1983) found a heteroclinic orbit of a similar type as we found in Fig. 10. For the full system (3.4), this heteroclinic loop yields an invariant spheroidal surface which must break-up under perturbation. Thus again, we expect horseshoe dynamics in the neighborhood of the limit cycle near the bifurcation.

6 Implication for general food chains

For the general family of food chain models, we obtain a normal form with the same terms having nonzero coefficients as we did for Hastings and Powell's model. Thus, we can do analysis for the more general models in precisely the same way which we did it for the particular food chain model, (3.4). The only difference is that parameters of the system (5.7) which we ultimately study will have different restrictions on magnitude and sign which depend on the functional response and density dependent effects. New types of dynamics can occur. For example, the het-

eroclinic loop shown in Fig. 10 may occur. The heteroclinic loop in Fig. 11 arises from (5.7) when $b < 0$. We remind the reader that $b < 0$ cannot occur for reasonable values of the original model parameters. Although this cannot apply to the food chain model (3.4), it certainly may apply to a more general predator-prey model. This would again imply horseshoe dynamics with a different shaped invariant set than ones found for the model (3.4).

We also want to compare (3.4) with the corresponding more general model, (2.4). The main question of interest is whether the form of the Holling type II functional response or the density dependent growth rate functions are important in determining the dynamics. We can compare the general models (3.4) by computing the coefficients in (2.7). The differences in magnitude and sign in these coefficients determines the ultimate normal form and subsequent analysis. Since we ultimately study dynamics in the rz-plane, we need not determine values for c_1, c_4, or c_5. The values for the remaining parameters, derived in Klebanoff (1992), are

$$c_2 = \frac{f_1'(f_1 f_2 - Df_2') - f_2[Df_1'' - f_1 D'']}{2f_1}, \tag{6.1}$$

$$c_3 = \frac{(f_1'' f_1 - (f_1')^2)[Df_1'' - f_1 D''] - f_1 f_1'[Df_1''' - f_1 D''']}{16D(f_1')^2}, \tag{6.2}$$

$$c_6 = \frac{(f_2)^2\{((f_1')^2 + 2f_1' f_2' + f_1 f_1'')[Df_1'' - f_1 D''] - f_1 f_1'[Df_1''' - f_1 D''']\}}{4(f_1)^2 f_1'}, \tag{6.3}$$

$$c_9 = \frac{Df_1' f_2'' - f_2'[Df_1'' - f_1 D'']}{4Df_1'}, \tag{6.4}$$

$$c_{10} = \frac{-(f_2)^2 f_2'[Df_1'' - f_1 D'']}{2(f_1)^2} \tag{6.5}$$

where D and f_1 are evaluated at $\bar{x}$ and f_2 is evaluated at $\bar{y}$. The recurring expressions in square brackets are positive for (3.4). One can see that there are many possible ranges for these parameters depending on the functional responses or the prey's growth rate.

We now consider what happens as density dependent effects are enhanced. As density dependent effects increase, $D(\bar{x})$ decreases in magnitude. We must still have $D(\bar{x}) > 0$ since the bottom species must have a positive net growth rate in order to remain in a non trivial equilibrium state. Furthermore, $D''(\bar{x})$ decreases from zero and thus increases in magnitude. Thus, the expression

$$[Df_1'' - f_1 D''] \tag{6.6}$$

becomes more positive as density dependent effects are enhanced. Since the expression (6.6) is negative when density dependent effects are absent, by continuity, the expression can be negative, zero, or positive. As a result, we see that there may be many other types of dynamics such as those shown in Fig. 11.

The role of varying the functional response is more complex. However, it is clear that by varying the functional response type, the signs and relative magnitudes of the coefficients, c_i, do change. We have not attempted to catalog the effects of different functional response types and density dependent effects.

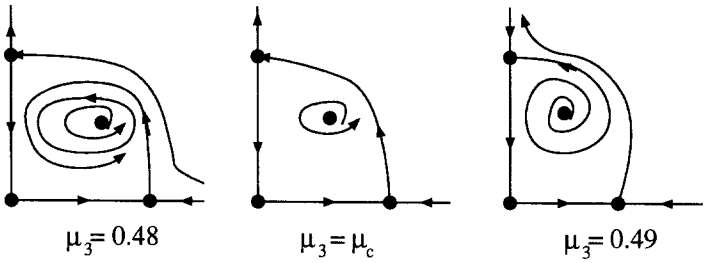

Fig. 11. If we let μ_3 be the bifurcation parameter with $a = -1, b = -1, c = 0, \mu_1 = 1, \mu_2 = -1$, a heteroclinic bifurcation occurs for μ_3 between 0.48 and 0.49

7 Conclusions

We have used an approach based on bifurcation theory to show the existence of chaotic dynamics in a class of biologically reasonable three species models. Although the presence of chaos in three species food chains was demonstrated quite unequivocally by the numerical work of Hastings and Powell (1991), the approach we have outlined here has substantial advantages. Although part of our analysis is numerical, the work presented here is the first to demonstrate clearly the presence of chaos for a class of reasonable continuous time ecological models, without the need to resort to simulations. This makes a much more compelling case for the ubiquity of chaotic dynamics in most food webs that will be observed in nature.

The work we have presented here suggests a number of important directions for future work, some of which we are pursuing. In particular, as we suggested in the introduction, one can extend the analysis here to other food webs, and we will present results for other three species models elsewhere. We are also using this approach to look at spatially coupled systems with two or more species, although the algebraic challenges become more complex.

Finally, the work we have presented here presents a mathematical challenge as well. Can our partial results for the bifurcation phenomenon we have studied here be completed? Is it possible to determine as complete an analysis for the case we study here as for the similar, but apparently simpler, codimension two case studied in Guckenheimer and Holmes (1983)? A more complete mathematical analysis would extend the range of ecological conclusions which can be drawn.

A The normal form calculation

We now will compute the normal form for the vector field in (3.4) about the fixed point,

$$(\bar{x}, \bar{y}, 0) = \left(\frac{d_1}{a_1 - b_1 d_1}, \frac{a_1 - b_1 d_1 - d_1}{(a_1 - b_1 d_1)^2}, 0 \right) \tag{A.1}$$

We refer the reader to Klebanoff (1992) for all of the fine details of the normal form calculation. To first degree, the normal form for (3.4) about $(\bar{x}, \bar{y}, 0)$ is

$$\dot{x} = \nu_1 x + \omega y + O(2)\,,$$

$$\dot{y} = -\omega x + v_1 y + O(2)\,,$$
$$\dot{z} = v_2 z + O(2)\,, \tag{A.2}$$

where

$$v_1 = \frac{-a_1 d_1 + b_1 d_1 (a_1 - b_1 d_1 - d_1)}{2a_1(a_1 - b_1 d_1)}\,, \tag{A.3}$$

$$\omega = \sqrt{\frac{d_1(a_1 - b_1 d_1 - d_1)}{a_1} - \left(\frac{b_1 d_1 (a_1 - b_1 d_1 - d_1) - a_1 d_1}{2a_1(a_1 - b_1 d_1)}\right)^2}\,, \tag{A.4}$$

and

$$v_2 = \frac{-(a_1 - b_1 d_1)^2 d_2 + (a_1 - b_1 d_1 - d_1)(a_2 - b_2 d_2)}{(a_1 - b_1 d_1)^2 + b_2(a_1 - b_1 d_1 - d_1)}\,. \tag{A.5}$$

The linear part of (A.2) is most degenerate when $v_1 = v_2 = 0$ which implies

$$d_1 = \frac{a_1(b_1 - 1)}{b_1(b_1 + 1)}\,,$$
$$d_2 = \frac{a_2(1 + b_1)^2}{b_2(b_1 + 1)^2 + 4a_1 b_1}\,. \tag{A.6}$$

Thus, (A.6) is a condition for which (3.4) undergoes a bifurcation of codimension greater than or equal to two. One should note that since all of the original parameters were assumed positive, (A.6) implies that

$$b_1 > 1\,. \tag{A.7}$$

Applying the constraints in (A.6) yields

$$\omega = \frac{\sqrt{a_1(b_1 - 1)}}{b_1\sqrt{1 + b_1}}\,, \tag{A.8}$$

and the fixed point (A.1) takes the form

$$(\bar{x}, \bar{y}, 0) = \left(\frac{b_1 - 1}{2b_1}, \frac{(b_1 + 1)^2}{4a_1 b_1}, 0\right) \tag{A.9}$$

at the bifurcation.

A normal form for *any* analytic vector field with Jacobian matrix

$$\begin{pmatrix} 0 & \omega & 0 \\ -\omega & 0 & 0 \\ 0 & 0 & 0 \end{pmatrix}\,, \tag{A.10}$$

is given by (2.5). Furthermore, the general family of food chain models (2.4) of which (3.4) is a member has a corresponding normal form given by (2.6) which can be conveniently written in cylindrical coordinates as shown in (2.7). While we refer the reader to Klebanoff (1992) for details of these calculations, we point out that normal form calculations are not unique. It is by careful choice of transformations

in the normal form calculation that makes (2.7) independent of θ. In fact, the vector field in (2.7) can be made independent of θ up to any degree (Wiggins 1990). Thus, we can study system (2.6) in the rz-plane. Furthermore, we will make only local arguments so that we may ignore higher order terms.

Therefore, the normal form for (3.4) which we will study (after truncating at third order and dropping the azimuthal term) is

$$\begin{aligned} \dot{x} &= \gamma_1 rz + \gamma_2 rz^2 + \gamma_3 r^3 , \\ \dot{z} &= \gamma_4 r^2 z + \gamma_5 z^3 , \end{aligned} \tag{A.11}$$

where

$$\gamma_1 = \frac{2a_1a_2b_2(b_1+1)^2}{[4a_1b_1 + b_2(b_1+1)^2]^2} - \frac{a_2(b_1^2-1)}{4a_1b_1 + b_2(b_1+1)^2} , \tag{A.12}$$

$$\gamma_2 = \frac{16a_1a_2^3b_1^3(b_1+1)^4}{[4a_1b_1 + b_2(b_1+1)^2]^4} - \frac{2a_2^2b_1(b_1+1)^3}{[4a_1b_1 + b_2(b_1+1)^2]^2} , \tag{A.13}$$

$$\gamma_3 = \frac{a_1b_1(b_1-1)}{2(b_1+1)^2} , \tag{A.14}$$

$$\gamma_4 = \frac{32a_1^3a_2b_1^3b_2}{[4a_1b_1 + b_2(b_1+1)^2]^3} - \frac{8a_1^2a_2b_1^3(b_1-1)}{(b_1+1)[4a_1b_1 + b_2(b_1+1)^2]^2} , \tag{A.15}$$

and

$$\gamma_5 = \frac{16a_1a_2^3b_1^3(b_1+1)^4}{[4a_1b_1 + b_2(b_1+1)^2]^4} . \tag{A.16}$$

Note that while the signs of γ_1 and γ_2 cannot be determined without further constraints, γ_3, γ_4 and γ_5 are strictly negative.

B Unfolding analysis

Isocline analysis of unfolded system

We begin by studying the nullclines of (5.7). Clearly, $r = 0$ and $z = 0$ are nullclines of $\dot{r} = 0$ and $\dot{z} = 0$ respectively. There are also non trivial nullclines. Corresponding to $\dot{r} = 0$ is the curve

$$\frac{4a^2}{1-4a\mu_1}\left(z + \frac{1}{2a}\right)^2 - \frac{4a}{1-4a\mu_1}r^2 = 1 \quad \text{if} \quad 1 - 4a\mu_1 \neq 0 , \tag{B.1}$$

or the pair of lines

$$z = \frac{-1}{2a} \pm \frac{1}{\sqrt{a}}r \quad \text{if} \quad 1 - 4a\mu_1 = 0 . \tag{B.2}$$

If $a > 0$, then (B.1) is a hyperbola. If $a < 0$ and $1 - 4a\mu_1 > 0$, then (B.1) is an ellipse. If $a < 0$ and $1 - 4a\mu_1 < 0$, then (B.1) has no solution set. Also, if $a = 0$, the parabola

$$z = r^2 - \mu_1 \tag{B.3}$$

is the r-nullcline. Corresponding to $\dot{z} = 0$ is the ellipse

$$\frac{4c^2}{\mu_3^2 + 4c\mu_2}\left(z - \frac{\mu_3}{2c}\right)^2 + \frac{4bc}{\mu_3^2 + 4c\mu_2} r^2 = 1 \quad \text{if} \quad \mu_3^2 + 4c\mu_2 > 0\,. \tag{B.4}$$

The curve in (B.4) has no solution set if $\mu_3^2 + 4c\mu_2 < 0$ and has only the point $(0, \mu_3/(2c))$ for a solution when $\mu_3^2 + 4c\mu_2 = 0$. The fixed points occur when a nullcline for r coincides with a nullcline for z. There are so many possible combinations of r and z nullclines possible, that we will not consider them all. Instead, we summarize the r and z components of flow separately.

We first take the non trivial elliptical z-nullcline. By sampling inside and out of the ellipse, one can easily show that inside the ellipse but in the first quadrant, trajectories must decrease in z. Biologically, this means that the highest trophic species population size is bounded. For the special case when $\mu_3^2 + 4c\mu_2 = 0$, the radius of the ellipse has shrunk to zero. If $\mu_3^2 + 4c\mu_2 < 0$, trajectories always decrease in z in the first quadrant.

The r-component of the vector field has more complications than the z-component since there are three conic sections rather than one to be concerned with. In the first quadrant, r-components of trajectories increase when inside the nullcline ellipse or hyperbola with vertical symmetry and decrease when outside. On the other hand, in the first quadrant, r-components of trajectories decrease when inside the hyperbola with horizontal symmetry and increase when outside. When the nullclines are absent, the flow decreases toward the axes. Figure 12 summarizes these results as well as the special case when the nullclines are lines.

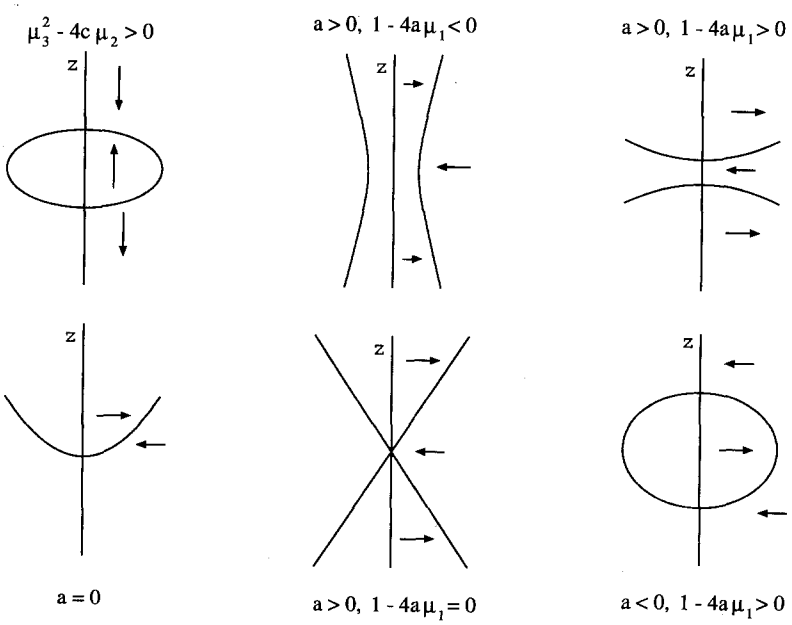

Fig. 12. The nullclines are symmetric about the z-axis. Arrows denote direction of flow in positive time component-wise. Arrows drawn are assumed to lie inside the first quadrant

The fixed points and stability

The fixed points of system (5.7) are $(0,0),(\sqrt{\mu_1},0),(0,\tilde{z}_i),(\hat{r}_1,\hat{z}_1)$, and $(\hat{r}_2,\hat{z}_2)$, where

$$\tilde{z}_i = \frac{\mu_3 + (-1)^{i-1}\sqrt{\mu_3^2 + 4c\mu_2}}{2c}, i = 1,2, \tag{B.5}$$

$$\hat{r}_i = \sqrt{\mu_1 + \hat{z}_i + a\hat{z}_i^2}, i = 1,2\,, \tag{B.6}$$

and

$$\hat{z}_i = \frac{-(b-\mu_3) + (-1)^{i-1}\sqrt{(b-\mu_3)^2 - 4(ab+c)(b\mu_1 - \mu_2)}}{2(ab+c)}, i = 1,2. \tag{B.7}$$

By linearization about these fixed points, conditions for local bifurcations are determined. Table 1 shows the eigenpairs for the fixed points lying on the axes. One should note that the origin is always a fixed point, and $(\sqrt{\mu_1},0)$ is another fixed point when $\mu_1 > 0$.

Due to the many parameters involved in the planar system (5.7), we are unable to perform a complete analysis. Fortunately, we are not interested in the typical dynamics of system (5.7), but instead, we want to show the types of bifurcations and invariant sets which arise from (5.7). This in turn will imply dynamics for the full system since the rz-plane can be thought of as a Poincaré section of the full system, and the dynamics of (5.7) are similar to a Poincaré map for the full system.

In order to obtain limit cycles in the full system (3.4), we must find at least one of the fixed points, $(\hat{r}_i,\hat{z}_i)$ in the positive quadrant. Fortunately, it is easy to prove that $(\hat{r}_i,\hat{z}_i)$ exists in the first quadrant. For example, if we require $\mu_1 > 0$ and $a > 0$, then clearly $\hat{r}_i > 0$ if $\hat{z}_i > 0$. Thus, we only need to furnish conditions for $\hat{z}_i > 0$. Choosing $0 < b < \mu_3$ and further choosing μ_1 and μ_2 so that $0 < b\mu_1 - \mu_2 < \varepsilon$ where ε is a small positive number, we are guaranteed two distinct values for $\hat{z}_i > 0$. We could also find conditions for which only one of the non trivial fixed points exist or even so that neither of them exist. Of couse, in terms of the full system, it is the cases involving the non trivial fixed points that is of most interest since they correspond to the limit cycles and ultimately chaos. While it is comforting that the unfolding does predict all of the simple behavior exhibited in the full model, here we will concentrate only on the more complicated behavior.

Table 1. The eigenpairs of the fixed points which lie on the rz-axes

	λ	x_1	λ_2	x_2
$(0,0)$	μ_1	$(1,0)$	μ	$(0,1)$
$(\sqrt{\mu_1},0)$	$-2\mu_1$	$(1,0)$	$\mu_2 - b\mu_1$	$(\sqrt{\mu_1}, \mu_2 + (2-b)\mu_1)$
$(0,\tilde{z}_i)$	$\mu_1 + \tilde{z}_i + a\tilde{z}_i^2$	$(1,0)$	$\mu_2 + 2\mu_3\tilde{z}_i - 3c\tilde{z}_i^2$	$(0,1)$

Some of the bifurcation behavior

The fixed points $(0,\tilde{z}_i)$ can undergo pitchfork bifurcations. We show this by applying the center manifold theory. We first move $(0,\tilde{z}_i)$ to the origin so that the system corresponding to (5.7) is

$$\begin{aligned}
\dot{r} &= \mu r + (1 + 2a\tilde{z}_i)rz + arz^2 - r^3, \\
\dot{z} &= (\mu_2 + 2\mu_3\tilde{z}_i - 3\tilde{z}_i^2)z - b\tilde{z}_i r^2 + (\mu_3 - 3c\tilde{z}_i)z^2 - br^2 z - cz^3, \\
\dot{\mu} &= 0\,,
\end{aligned} \tag{B.8}$$

where $\mu = \mu_1 + \tilde{z}_i + a\tilde{z}_i^2 = 0$ is the bifurcation value. By the center manifold theorem, we know that a graph of the local center manifold is locally represented by $z = h(r,u)$ where $h(0,0) = 0$ and $Dh(0,0) = 0$. Thus, we assume that

$$h(r,\mu) = \alpha_1 r^2 + \alpha_2 \mu r + \alpha_3 \mu^2 + O(3) \tag{B.9}$$

where $h(r,\mu)$ satisfies

$$\begin{aligned}
D_r h(r,\mu)(\mu r + (1 + 2a\tilde{z}_i)rh(r,\mu) + arh^2(r,\mu) - r^3) \\
- (\mu_2 + 2\mu_3\tilde{z}_i - 3c\tilde{z}_i^2)h(r,\mu) \\
+ b\tilde{z}_i r^2 - (\mu_3 - 3c\tilde{z}_i)h^2(r,\mu) \\
+ br^2 h(r,\mu) + ch^3(r,\mu) = 0\,.
\end{aligned} \tag{B.10}$$

Substituting (B.9) into (B.10) and equating coefficients of like terms in μ and r yields

$$z = r^2 + O(3)\,. \tag{B.11}$$

Thus, on the center manifold of $(0,\tilde{z}_i)$, the dynamics are equivalent to

$$\dot{r} = \mu r + 2a\tilde{z}_i r^3 + O(4)\,. \tag{B.12}$$

Therefore, there is indeed a pitchfork bifurcation at $(0,\tilde{z}_i)$ with $\mu = 0$. If $a > 0$, the bifurcation is subcritical and if $a < 0$ the bifurcation is supercritical. Figure 13 shows the corresponding bifurcation diagrams. As a result of the bifurcation, one of the fixed points $(\hat{r}_i,\hat{z}_i)$ moves into the first quadrant. We remind the reader that this must correpond to a Hopf bifurcation in the positive octant about one of the fixed points, $(\hat{x}_i,\hat{y}_i,\hat{z}_i)$. Thus, while this is one of the simpler bifurcations which can occur, it demonstrates that a Hopf bifurcation occurs off of the non trivial fixed point in the positive octant. This is following by a period doubling route to chaos just as we observed. We next turn to the Hopf bifurcations in the plane which imply quasi-periodicity for the full system.

Hopf bifurcations can only occur off of the axes at one of the non trivial fixed points, $(\hat{r}_i,\hat{z}_i)$. We want to apply the Hopf Bifurcation Theorem to show that the bifurcation does occur and to determine the nature of the bifurcation.

Theorem B.1. *The Hopf Bifurcation Theorem (Wiggins 1990) Let the system* $\dot{x} = f_\mu(x), x\varepsilon\mathcal{R}^2, \mu\varepsilon\mathcal{R}$ *have an equilibrium at* $x = x_0$ *when* $\mu = \mu_0$. *If*

1) $D_x f_{\mu 0}(x_0)$ *has a simple pair of pure imaginary eigenvalues* $\lambda(\mu_0), \overline{\lambda(\mu_0)}$; *and*
2) $\frac{d}{d\mu}(Re(\lambda(\mu))\Big|_{\mu-\mu_0} \neq 0,$

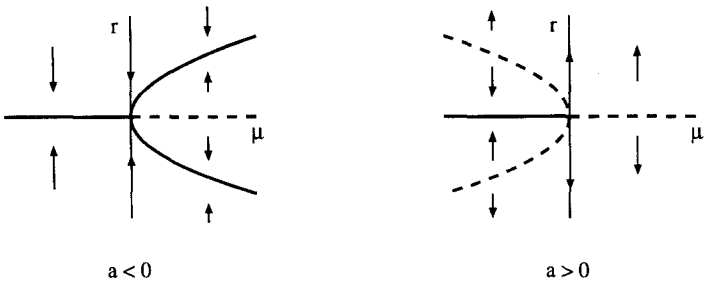

Fig. 13. When $a > 0$, the bifurcation is subcritical. When $a < 0$, the bifurcation is supercritical. *Dashed curves* correspond to unstable fixed points, while the *solid curves* correspond to stable fixed points

then a normal form for $\dot{x} = f_\mu(x)$ *about* $x = x_0$ *in polar coordinates is*

$$\begin{aligned} \dot{r} &= \delta(\mu - \mu_0)r + \alpha r^3 + O(5) \\ \dot{\theta} &= \omega + \gamma(\mu - \mu_0) + \beta r^2 + O(3) \end{aligned} \tag{B.13}$$

where

$$\omega = \mathrm{Im}(\lambda(\mu_0))\,, \tag{B.14}$$

$$\gamma = \frac{d}{d\mu}\left(\mathrm{Im}(\lambda(\mu))\right)\Big|_{\mu=\mu_0}\,, \tag{B.15}$$

$$\delta = \frac{d}{d\mu}\left(\mathrm{Re}(\lambda(\mu))\right)\Big|_{\mu=\mu_0}\,, \tag{B.16}$$

and α *and* β *are determined from the higher order terms in the Taylor expansion of* $f_\mu(x)$.

One should note that ω, β, and γ only affect the rotation speed of the flow near bifurcation, so that only δ, μ, and α have any role in determining the bifurcation. Thus, there are only four possibilities for bifurcation diagrams for (B.13). By applying fixed point analysis to the r-equation in (B.13), we find the fixed points $r = 0$ and $r = \sqrt{(-\delta/\alpha)(\mu - \mu_0)}$. If $\alpha\delta > 0$, then limit cycles are formed for $\mu < \mu_0$. When the bifurcating limit cycles are stable (i.e., $\alpha < 0$), the bifurcation is called *supercritical*, and when they are unstable, the bifurcation is called *subcritical*.

We can also determine the stability of the limit cycles. We note that

$$\frac{d}{dr}\left(\delta(\mu - \mu_0)r + \alpha r^3\right)\Big|_{r=\sqrt{(-\delta/\alpha)(\mu-\mu_0)}} = -2\delta(\mu - \mu_0). \tag{B.17}$$

We further note that limit cycles exist only if

$$\alpha\delta(\mu - \mu_0) < 0\,. \tag{B.18}$$

So, if $\alpha < 0$, then $\delta(\mu - \mu_0) > 0$. Thus, by (B.17), the limit cycles are stable when $\alpha < 0$. Similarly, we see that $\alpha > 0$ implies that $\delta(\mu - \mu_0) < 0$. Thus, the limit cycles are unstable when $\alpha > 0$.

We determine that the Hopf bifurcation occurs by choosing its location and applying the necessary conditions. We'll assume that the Hopf bifurcation occurs at $(\hat{r}_1, \hat{z}_1) = (1, 1)$. Then, since $(1, 1)$ is fixed, we must have

$$\mu_1 = -a\,, \tag{B.19}$$

$$\mu_2 = b + c - \mu_3\,. \tag{B.20}$$

Also, for a Hopf bifurcation to occur, the real part of the eigenvalues of the Jacobian matrix must go through zero while the imaginary part of the eigenvalues remain nonzero. Thus, the trace of the Jacobian at the fixed point must be zero and the determinant of the Jacobian at equilibrium must be positive, that is

$$\operatorname{tr} J(1,1) = 0\,, \tag{B.21}$$

$$\det J(1,1) > 0\,. \tag{B.22}$$

These two conditions along with (B.19) and (B.20) yield the following four necessary conditions for the Hopf bifurcation to occur.

$$\mu_1 = -a\,, \tag{B.23}$$

$$\mu_2 = b - c - 2\,, \tag{B.24}$$

$$\mu_3 = 2c + 2\,, \tag{B.25}$$

$$2ab + b - 2 > 0\,. \tag{B.26}$$

To determine the stability of the limit cycles formed or even whether or not a degenerate Hopf bifurcation occurs (i.e., the third degree terms in the normal form are absent), we study the normal form of the vector field (5.7) subject to (B.23)-(B.26). We move (1, 1) to the origin by the transformation

$$\begin{pmatrix} r \\ z \end{pmatrix} \to \begin{pmatrix} r-1 \\ z-1 \end{pmatrix} \tag{B.27}$$

and use the necessary conditions for a Hopf bifurcation. This yields the system

$$\begin{pmatrix} \dot{r} \\ \dot{z} \end{pmatrix} = \begin{pmatrix} -2 & 1+2a \\ -2b & 2 \end{pmatrix} \begin{pmatrix} r \\ z \end{pmatrix} + \begin{pmatrix} (1+2a)rz + az^2 - 3r^2 + arz^2 - r^3 \\ (2-c)z^2 - br^2 - 2brz - br^2 z - cz^3 \end{pmatrix}. \tag{B.28}$$

We now introduce the linear transformation

$$\begin{pmatrix} r \\ z \end{pmatrix} = \begin{pmatrix} -2 & -\sqrt{4ab+2b-4} \\ -2b & 0 \end{pmatrix} \begin{pmatrix} u \\ v \end{pmatrix} \tag{B.29}$$

to system (B.28) to yield

$$\begin{pmatrix} \dot{u} \\ \dot{v} \end{pmatrix} = \begin{pmatrix} 0 & -\sqrt{4ab+2b-4} \\ \sqrt{4ab+2b-4} & 0 \end{pmatrix} \begin{pmatrix} u \\ v \end{pmatrix} + \begin{pmatrix} f(u,v) \\ g(u,v) \end{pmatrix} \tag{B.30}$$

where

$$f(u,v) = 2(1+bc)u^2 - 4b(1+bc)u^3 + 2s(1+b)uv - 4bsu^2v + \frac{4ab+2b-4}{2}v^2 - b(4ab+2b-4)uv^2, \quad \text{(B.31)}$$

$$g(u,v) = \left(-2s - \frac{4b}{s}(ab+c)\right)u^2 + \left(2s + \frac{4b}{s}(1+2bc)\right)u^3 + (8-6b-4ab)uv + (4ab^2+8b-12)u^2v + 2sv^2 + (-6s+2bs)uv^2 - (4ab+2b-4)v^3, \quad \text{(B.32)}$$

and

$$s = \sqrt{4ab+2b-4}\,. \quad \text{(B.33)}$$

To determine the stability of the limit cycles formed in the bifurcation, rather than completing the normal form calculation about (1, 1), we use the fact (derived in Guckenheimer and Holmes 1983) that

$$\alpha = \frac{1}{16}\left(f_{uuu} + f_{uvv} + g_{uuv} + g_{vvv} + \frac{1}{s}\left(f_{uv}(f_{uu}+f_{vv}) - g_{uv}(g_{uu}+g_{vv}) - f_{uu}g_{uu} + f_{vv}g_{vv}\right)\right)\Big|_{(u,v)=(0,0)}\,. \quad \text{(B.34)}$$

We further let $a = b = c = 1$ and note that this satisfies (B.26). Then, upon computing α in (B.34), we find that $\alpha = 4$. Also, since $\delta = 1/2$, the bifurcation is *sub*critical with *unstable* limit cycles.

Acknowledgement. We thank John Guckenheimer for his thoughtful comments and suggestions. Also of great help were the comments made by Tom Powell and John Hunter. We are gracious for the insight that Bill Vance offered during the course of this work. We also are grateful for the wonderful facilities at the Institute of Theoretical Dynamics. This work was supported partially by grant DE-FG03-89ER60886/A000 to AH from the Ecological Research Division, Office of Health and Environmental Research, US Department of Energy. This support does not constitute an endorsement of the views expressed here.

References

1. Gilpin. M. E.: Spiral chaos in a predator-prey model. Am. Nat. **113**, 306–308 (1979)
2. Guckenheimer, J.: Holmes, P.: Nonlinear Oscillations, Dynamical Systems, and Bifurcations of Vector Fields. (Appl. Math. Sci., Vol. 42) Berlin, Heidelberg, New York: Springer 1983.
3. Hastings, A.: Powell, T.: Chaos in a three-species food chain. Ecology **72**(3), 896–903 (1991)
4. Klebanoff, A.: Chaos in three species food chains. PhD thesis. University of California, Davis, June 1992
5. Pimm, S. L.: Food Webs. London: Chapman and Hall 1982
6. Rosenzweig, M. L.: Exploitation in three trophic levels. Am. Nat. **107**, 275–294 (1973)
7. Steele, J. H.: Henderson, E. W.: The role of predation in planktaon models. J. Plankaton Res. **14**(1) 157–172 (1992)
8. Wiggins, S.: Introduction to Applied Nonlinear Dynamical Systems and Chaos. (Texts Appl. Math, Vol. 2) Berlin, Heidelberg, New York: Springer 1990
9. Wollkind, D. J.: Exploitation in three trophic levels: an extension allowing intraspecies carnivore interaction. Am. Nat. **110**, 431–447 (1976)